OPEN ACCESS
IOP Publishing
Modelling and Simulation in Materials Science and Engineering
Modelling Simul. Mater. Sci. Eng. **32** (2024) 075008 (16pp) https://doi.org/10.1088/1361-651X/ad6ea8

A model for the precipitate transformation of Mg–Si-rich clusters into Mg_5Si_6 β'' in Al–Mg–Si aluminum alloys

Y V Shan[1,*], A Redermeier[2,3], R Kahlenberg[1,2] and E Kozeschnik[1]

[1] Institute of Materials Science and Technology, TU Wien, Getreidemarkt 9, 1060 Vienna, Austria
[2] Materials Center Leoben Forschung GmbH, Peter Roseggerstraße 13, 8700 Leoben, Austria
[3] Now: TGM, Wexstraße 19-23, 1200 Vienna, Austria

E-mail: yao.shan@tuwien.ac.at

Received 25 January 2024; revised 11 June 2024
Accepted for publication 13 August 2024
Published 3 September 2024

Abstract

A model is developed that describes the kinetics of precipitate transformations in the course of natural and artificial aging of Al alloys containing Mg and Si additions. In our approach, the disordered Mg–Si-rich clusters, which form during natural aging in the highly supersaturated Al matrix, can directly transform into the monoclinic Mg_5Si_6 (β''), without prior dissolution of the clusters and independent nucleation of β'' in the Al matrix. The transformation rate is evaluated with classical nucleation theory (CNT), assuming that the clusters represent an infinitely large matrix phase in which the β'' precipitates can nucleate. The adapted CNT model is described, and the basic features of the precipitate transformation are discussed in a parameter study. The model can also account for the observation that, during natural aging, the parent clusters occur in a variety of Mg to Si ratios, all of which have a characteristic probability of either transforming into the β'' phase or dissolving.

Keywords: precipitate transformation, β'' kinetics, Al–Mg–Si alloys

* Author to whom any correspondence should be addressed.

1. Introduction

In the past decades, substantial progress has been made in the understanding of the mechanisms underlying the precipitation sequence in 6xxx-Al alloys. When heat treating these alloys after solutionizing and quenching to room temperature, the typical (simplified) sequence is [1]

SSSS -> **Mg–Si-rich clusters ->** $\boldsymbol{\beta''} -> \beta' -> \beta$,

where SSSS is the supersaturated solid solution, β'' (monoclinic Mg_5Si_6 [2, 3]) and β' (hexagonal $Mg_{1.8}Si$ [4, 5]) are precursor phases to the stable β phase (cubic Mg_2Si). The term *Mg–Si-rich clusters* above summarizes any early structures that precede β'' and do not yet qualify as a *precipitate*.

It is well-known that these early structures forming from SSSS directly affect the precipitation of β'' and hence the artificial aging response (see e.g. [6]). The fact that different alloy compositions and heat treatments lead to different cluster compositions which in turn have differing thermal stabilities was demonstrated, for instance, by Poznak *et al* [7]. In addition to chemistry variations, short-range ordering and defect structures were postulated to play a part in the transformation of early precursors into β'' (see, e.g. [8, 9]). A recent investigation on the transformation of clusters and GP-zones into β'' by Marioara *et al* [10], using transmission electron microscopy as well as density functional theory (DFT), confirmed all aforementioned points. They find a variety of early structures forming from SSSS and categorize them into (i) *face-centered-cubic* (FCC) structures and (ii) *other* structures which incorporate, for instance, certain interstitial defects and vacancies. The FCC variants occur with a wide range of chemical compositions while the others tend to be closer to the composition and structure of β''. The complementary DFT calculations presented therein further show that (i) any considered structure with a composition close to that of β'' tends to be more stable and (ii) the additional incorporation of defects further increases the stability. The authors also observe individual β'' columns (called *eyes* in [10]) occurring *within* compositionally similar FCC structures and conclude that the latter may indeed serve as nucleation sites for β''. They mention that the transformation requires only a *thermally activated* jump of atoms into an octahedral site.

While some of the aforementioned experimental findings are comparably new [10], modeling of the precipitation processes during aging of 6xxx alloys has been reported several times beforehand [11–18]. Bratland *et al* [11] developed a model for isothermal and continuous heat treatments in the framework of the Johnson–Mehl–Avrami–Kolmogorov (JMAK) approach and applied it to various steps in the processing of an extruded Al-6082 alloy. Khan *et al* [12] developed a model for precipitation strengthening in 6xxx alloys based on the Kampmann Wagner numerical (KWN) approach. Esmaeili *et al* [13] modeled the influence of natural aging on the artificial aging response at 'high' temperatures with a JMAK approach assuming only cluster dissolution. They observe increasingly large deviations from experimental data at lower artificial aging temperatures and relate those to a missing transformation mechanism. Milkereit and Starink [14] presented a model for the prediction of differential scanning calorimetry (DSC) experiments, demonstrating the potential of numerical simulation in identifying precipitation reactions measured with DSC. Myhr *et al* [15, 16] developed a simulation framework for the prediction of the yield strength during the natural and artificial aging of 6xxx aluminum alloys. Lang *et al* [17, 18] applied the thermokinetic software package MatCalc [19] to describe the entire precipitation sequence in the simulation of continuous heating DSC experiments for 6xxx and 7xxx aluminum alloys. Several other models related to aluminum technology have recently been reviewed by Raabe *et al* [20].

Despite the wide variety of computational efforts to describe the evolution of precipitates in Al alloys, the existing approaches have in common that, either, the clusters and precipitates are treated as unconnected and independent objects in the sense of the KWN approach. Or, the phase fractions of a sequence of precipitation events are described by some statistical theory, where one phase grows at the expense of a precursor phase, however, without consideration of the underlying transformation mechanism. As of now, there is no approach to describe the nucleation/transformation of precursor precipitates into beta DP in dependence of their composition and size.

To fill this gap, in the present work, a novel methodology is developed to model the evolution of (disordered) Mg–Si-rich clusters into (ordered) crystalline Mg_5Si_6 precipitates as a *direct precipitate transformation* within the MatCalc framework. This means that the β'' precipitates nucleate and grow directly within the precursor cluster phase, independent from the surrounding Al matrix—in contrast to previous approaches and in alignment with state-of-the-art experimental investigations [10]. It is emphasized that defects or ordering within clusters are not *explicitly* considered i.e. the model uses disordered clusters with the same face-centered cubic structure as the Al matrix to approximate any precursor structure to the β'' phase [21]. However, it will be shown that regardless of this simplification, the model presented allows to (i) model variations in the transformation probability of a cluster based on differences in chemical composition, i.e. thermodynamic stability and (ii) do so via a thermally activated process that is independent of the surrounding Al matrix [22]. This directly relates the cluster chemistry and size to the probability of a 'transformation event' and offers the possibility to model a gradual change from heat treatments governed by cluster dissolution (e.g. during artificial aging at high temperatures) to those dominated by cluster transformation (e.g. during artificial aging at lower temperatures).

2. The model

The starting point of our modeling is a pre-existing size distribution of Mg–Si-rich clusters, which is assumed to be present after some hypothetical solutionizing, quenching, and natural aging heat treatment of an Al-alloy with a nominal composition of 1 at% Mg and 1 at% Si. Within the MatCalc (http://matcalc.at) framework, the distribution is initialized such that all clusters have an identical composition of 0.45 Mg and 0.55 Si (in mole fraction). The number densities and radii are set such that the cluster phase fraction corresponds approximately to its phase fraction in metastable equilibrium with the Al matrix and the radii are in the order of magnitude of typical cluster sizes after natural aging [22–24]. As a consequence, the independent nucleation of β'' precipitates is suppressed and the only possible formation mechanism for β'' is the direct precipitate transformation from the clusters. The thermodynamic and diffusion information is acquired from suitable databases according to the CALPHAD framework [25]. It is then assumed that

1. The β'' precipitates nucleate inside the cluster volume,
2. Classical nucleation theory (CNT) can be applied to evaluate the transformation rate,
3. Nucleation becomes possible if the cluster exceeds a certain critical size, such that the atoms in the cluster are sufficient to build the β'' precipitate,
4. The nucleation criterion is applied as a 'soft' criterion, meaning that clusters, which are smaller than the prescribed critical size, can still transform with a certain probability,
5. The transformation completes instantaneously after nucleation,

6. Exactly the amount of atoms in the cluster, which is needed to form the β'' precipitate, is transferred from the cluster into the newly formed β'' precipitate,
7. The excess Si or Mg atoms from the cluster are released into the surrounding matrix to maintain mass balance.

The first assumption is an original aspect of the present model but also backed by recent experimental results [10]. The second assumption is related to the fact that for thermally activated nucleation events in a KWN approach (as used by MatCalc), there are currently no eligible alternatives. Similar arguments have been raised by other authors [15]. The third assumption relates to the fact that building the unit cell of β'' requires a minimum number of Mg and Si atoms, which depends on chemistry and size of the cluster. The fourth criterion relates to the fact that β'' may occur with varying compositions [26] and the strict stochiometric criterion used to calculate the critical radius would probably underestimate the number of transformations. Criteria 5–7 are more or less a necessity, since it is not feasible to consider *partially* transformed clusters with a residual FCC component in the simulations. The error introduced by this *instant dissolution* should be small, since clusters with disadvantageous chemistry seldomly transform in the first place [10].

The simulation methodology, otherwise, follows the one developed earlier in the MatCalc simulation framework [27–29].

2.1. Nucleation rate

In solid-state CNT, the transient nucleation rate, J, for a precipitate is commonly expressed as, e.g. [30],

$$J = N_0 Z \beta^* \exp\left(\frac{G^*}{k_\mathrm{B} T}\right) \exp\left(-\frac{\tau}{t}\right), \tag{1}$$

with N_0 being the number of potential nucleation sites, Z the Zeldovich factor, β^* the atomic attachment rate onto the critical nucleus, G^* the critical nucleation energy and τ the incubation time. The individual terms are evaluated as

$$Z = \left[\frac{-1}{2\pi k_\mathrm{B} T} \frac{\partial^2 \Delta G}{\partial n^2}\right]^{\frac{1}{2}}, \tag{2}$$

with ΔG being the nucleation energy and n the number of atoms in the critical nucleus,

$$\beta^* = \frac{4\pi \rho^{*2}}{a^4 \Omega} \left[\sum_{i=1}^{j} \frac{(c_{ki} - c_{0i})^2}{c_{0i} D_{0i}}\right]^{-1}, \tag{3}$$

with ρ^* being the critical nucleation radius, Ω the atomic volume, c the concentration in the precipitate k and the matrix, 0, respectively, j the number of elements, and D the diffusion coefficients. The nucleation barrier is

$$G^* = \frac{16\pi}{3} \frac{\gamma^3}{d_m^2}, \tag{4}$$

with the chemical driving force, d_m, and the interfacial energy, γ, and

$$\tau = \frac{1}{2\beta^* Z^2}. \tag{5}$$

In conventional precipitation kinetics modeling, the thermodynamic and kinetic quantities entering the nucleation rate equation are evaluated with respect to the Al matrix. In the present modeling approach, the nucleus of β'' is assumed to form inside a pre-existing Mg–Si-rich cluster. Therefore, all thermodynamic and kinetic properties are evaluated with respect to the cluster phase instead of the Al matrix. In this sense, the cluster phase is assumed to represent an infinitely large chemical environment, in which the nucleation event of the β'' precipitate occurs. The relevant quantities, e.g. the chemical potentials, driving forces, as well as diffusion coefficients, are consequently all derived from the properties of the cluster phase.

In order to be able to acquire these properties, appropriate thermodynamic and kinetic databases must be available. In the present work, the assessment of Povoden-Karadeniz *et al* [31] is used. In this CALPHAD modeling, the thermodynamic description of the cluster phase (CL_MGSI) allows for the calculation of all respective quantities. The diffusion kinetics inside the cluster is assumed to be identical to the one of the Al matrix, in the absence of corresponding experimental information.

2.2. Minimum transformation radius

In the nucleation model outlined before, the procedure for evaluating the number of potential nucleation sites, N_0, has not yet been specified. In contrast to homogeneous nucleation in CNT, where every atom in the unit volume is assumed to represent a potential nucleation site, the number of sites supporting the precipitate transformation is limited to the number of atoms in the parent (cluster) precipitates of sufficient size, which can build up the product precipitate, β''. In the practical simulation, the nucleation rate for the precipitate transformation from clusters to β'' is evaluated and stored individually for each cluster size distribution record [28]. This value is then used to calculate the number of parent precipitates (clusters) that will transform into the product phase (β'') in each time interval of the numerical integration procedure. The detailed algorithm describing the 'smooth' size class-related nucleation rates is outlined, next.

In the first step, a prescribed minimum nucleation radius, $r_{\mathrm{min,nucl}}$, is introduced as the limit above which the parent precipitate is assumed to be sufficiently large to be a potential source of nucleation. In the second step, the 'effective' (reduced) radius of the size class is adapted such that only the number of atoms is accounted for that can build up the product precipitate with given chemical composition. This reduced (effective) radius is denoted as r_{eff}. If the effective radius exceeds the minimum nucleation radius, all atoms in the precipitates of the size class are counted as potential nucleation sites to determine N_0 in equation (1). Only one single β'' precipitate can nucleate in one cluster precursor.

In practical simulations, this 'hard' criterion has shown to be problematic because of rather steep changes in the nucleation rate once a size class with a high number of precipitates switches from under-critical to over-critical size. For this reason, a 'soft' criterion is used, which allows a certain portion of under-critical precipitates also to contribute to the available number of potential nucleation sites. With the scaled radius,

$$\bar{r} = \frac{r_{\mathrm{min,nucl}} - r_{\mathrm{eff}}}{r_{\mathrm{eff}}} \tag{6}$$

a factor f_{nucl} can be defined with

$$f_{\mathrm{nucl}} = \exp\left(-\frac{(\bar{r})^m}{\sigma^2}\right), \text{ for } r_{\mathrm{eff}} \leqslant r_{\mathrm{min,nucl}}, \tag{7}$$

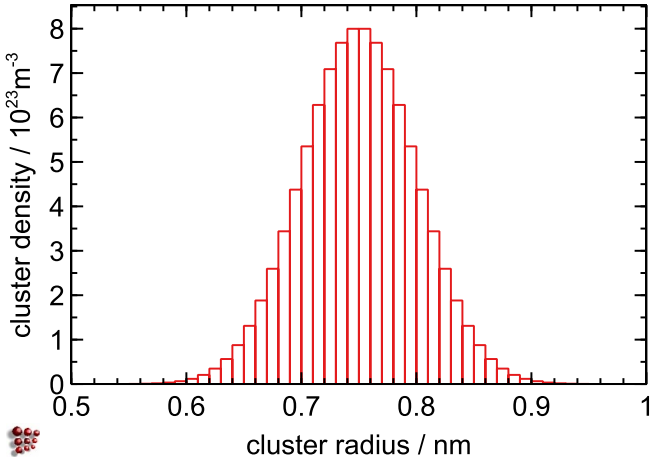

Figure 1. Initial normal distribution of 0.45 Mg–0.55 Si-clusters before the start of the precipitate transformation of clusters into β''.

as the number fraction of under-critical precipitates of a certain size class that contributes to the number of potential nucleation sites although their class radius is below $r_{\mathrm{min,nucl}}$. Note that $\bar{r}$ can adopt values between 0 and 1, since r_{eff} is always smaller or equal to $r_{\mathrm{min,nucl}}$. The coefficients are used with $m = 1$ and $\sigma = 0.15$, in the present work. Finally, the total number of nucleation sites, N_0, is given by the sum of contributions of size classes k as

$$N_0 = \sum_{k=0}^{n} f_{\mathrm{nucl},k}\, N_k \frac{V_{\mathrm{prec,eff},k}}{V_{\mathrm{atom}}} \tag{8}$$

with N_k being the number of precipitates in class k, $V_{\mathrm{prec,eff}}$ the effective precipitate volume and V_{atom} the atomic volume of Al.

For the simulations, the initial size distribution of parent precipitates with 0.45 Mg and 0.55 Si (mol fraction), i.e. clusters, is defined as the normal distribution of clusters with a minimum radius of 0.5 nm, a mean radius of 0.75 nm, and a maximum radius of 1.0 nm. The standard deviation is set to 0.05, which leads to the size distribution shown in figure 1.

Based on this distribution, the impact of the factor f_{nucl} is investigated in figure 2 (circle symbols). If the minimum critical nucleation radius is set to small values, e.g. 0.6 nm, almost all precipitates in the distribution contribute to the number of potential nucleation sites for the transformation. With the increasing value of $r_{\mathrm{min,nucl}}$, continuously fewer precipitates are considered to be over-critical in the 'smooth' nucleation criterion and the nucleation rate thus drastically decreases. For comparison, the steady-state nucleation rate evaluated with the 'hard' criterion is also shown figure 1 (cross symbols). The numbers refer to the minimum/mean/maximum radius of the distribution as well as the standard deviation. Additionally, the hard criterion is evaluated for a narrower distribution (diamond symbols), showing the differences between soft and hard criterion become significantly more pronounced for narrow size distributions. The soft criterion for the narrow distribution is not shown since it is almost identical to the one for the wider distribution. Note that the steady-state nucleation rates do not converge at low values for the minimum nucleation radius. This is due to the different weights that are assigned to each size class and the interplay with the effective nucleation radius.

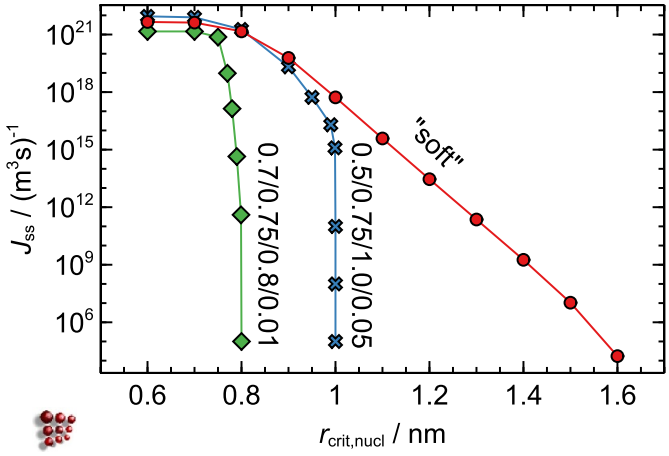

Figure 2. Steady-state precipitate transformation nucleation rate, J_{ss}, of clusters into β'' at 25 °C, showing the impact of the prescribed minimum nucleation radius for β'', calculated for the distribution shown in figure 1 ('soft'). For the other lines, see text.

3. Simulation

The present thermodynamic and kinetic simulations are carried out with the software package MatCalc [19] (http://matcalc.at) for a hypothetical 6xxx Al-alloy with a chemical composition of Al−1%Mg−1%Si (at%). The phases included in the simulations comprise the Al matrix (CALPHAD phase name: FCC_A1), the Mg–Si-rich clusters (CL_MGSI) and the Mg_5Si_6 β'' precipitates (MG5SI6_B_DP). The thermodynamic and diffusion data are taken from the open databases mc_al.tdb (version 2.035) and mc_al.ddb (version 2.004), which are published under the open database license (http://opendatacommons.org/licenses/odbl/1.0/) and are freely available on the MatCalc website (http://matcalc.at). The relevant thermodynamic modeling of these phases is reported in detail in Povoden-Karadeniz *et al* [31]

In the MatCalc simulations, the precipitation domain (al_matrix) is used with all default values for the FCC_A1 CALPHAD phase. Unlike in other simulations in Al alloys, no dynamic evolution of excess vacancies [32, 33] is considered here due to the benefit of a clear interpretation of the results. It is assumed that the equilibrium concentration of thermal vacancies is present, which means that the diffusion coefficients are taken as defined in the mobility database mc_al. The impact of this simplification is marginal, anyway, since the simulations are started with a close-to-equilibrium distribution of clusters that evolve into β'' in the direct precipitate transformation mode. This mechanism is not dependent on the number of excess vacancies in the Al matrix, since no long-range diffusion of atoms is necessary for it. The diffusion coefficients inside the clusters, which are required for the evaluation of the atomic attachment rate, are assumed to be identical to the standard diffusion coefficients in the Al matrix due to a lack of experimental data. The settings for the precipitate phases are summarized in table 1. All other parameters are left on their MatCalc default values and settings.

The calculation of interfacial energy in MatCalc modeling is commonly performed with the generalized broken bond model [34], including the size [35] and diffuse interface effects [36]. In the present work, only the size effect is used for the clusters, which is, for the current modeling not of relevance because the simulation is started with a prescribed cluster distribution.

Table 1. MatCalc simulation settings for precipitate phases.

	Clusters	β''
CALPHAD phase name	CL_MGSI	MG5SI6
# of size classes	250	250
Nucleation sites	Bulk	CL_MGSI
Nucleation model[a]	CNT	PT
Interfacial energy	Automatic (from GBB)[b]	0.1 J m^{-2}
Driving force[c]	From matrix	From parent

[a] CNT … Classical nucleation theory (nucleation inside Al matrix; PT … Precipitate transformation.
[b] From generalized broken bond (GBB) model [34] including the size [35] and diffuse interface [36] effect.
[c] With this setting, all thermodynamics and kinetics are evaluated from within either matrix or parent (clusters).

For the interfacial energy of β'' inside the cluster phase, an 'equivalent interfacial energy' is used with a constant value of 0.1 J m^{-2}. This has been done because the evaluation of interfacial energies requires rather accurate thermodynamics of the parent phase, which is available in the FCC_A1 phase, based on a vast richness of thermodynamic data existing for a multi-component Al matrix. For the cluster phase, the thermodynamic CALPHAD parameters have been evaluated for a solution of clusters inside Al. They do, unfortunately, not provide accurate enough data for β'' in clusters, at least not for the stability range at the fringes of Mg to Si ratios. It is therefore preferred, to use a constant value instead.

4. Results

With the previously outlined transformation model and simulation settings, the precipitate transformation of clusters into β'' precipitates is investigated.

4.1. Thermodynamics

First, the chemical driving forces for the formation of clusters and β'' within the Al matrix are shown in figure 3 for temperatures between 25 °C and 250 °C. In the figure, the Mg to Si ratio is varied between 0 and 1 mole fraction (mf). At room temperature, and based on the thermodynamic information used in the present study, the stability range of clusters is confined between 0.2 and 0.9 mf Mg, indicated by a positive value of the chemical driving force. At higher temperatures, the stability range becomes narrower, until it extends between only 0.47 and 0.63 mf at 250 °C. All clusters outside this range have a negative driving force and they are, therefore, not thermodynamically stable. The chemical driving force for β'' precipitation is shown as individual values at the stoichiometry of Mg_5Si_6, since the β'' phase is modeled as a line compound in the mc_al database. The Mg_5Si_6 phase is stable at all temperatures in the calculation.

The chemical driving force for the precipitate transformation, i.e. the direct transformation of clusters into β'', is evaluated with standard methods. Since the chemical composition of clusters and β'' is different, in general, the driving force for the precipitate transformation cannot simply be calculated as the difference of Gibbs energy of the two phases that are

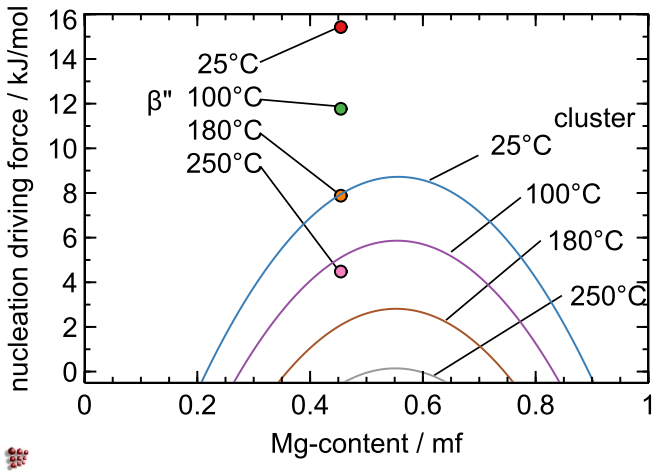

Figure 3. Chemical driving forces for Mg–Si-rich cluster and β'' precipitation in a supersaturated Al matrix at 25 °C, 100 °C, 180 °C and 250 °C as a function of Mg to Si ratio of the precipitates.

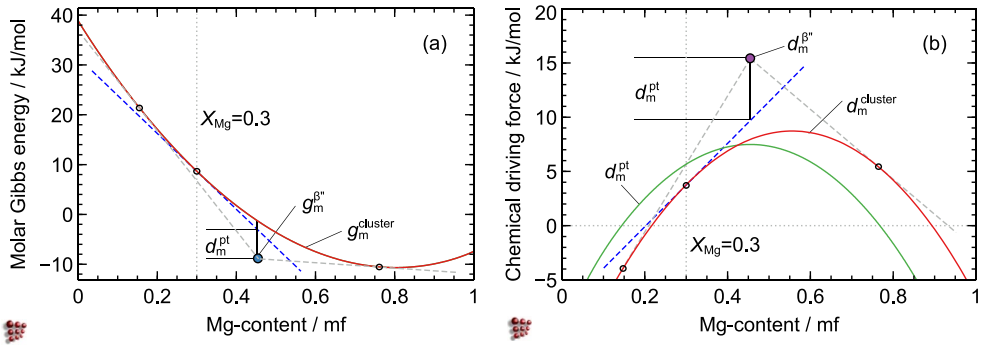

Figure 4. Construction of chemical driving forces (d_m^{pt}) for the precipitate transformation of Mg–Si-rich clusters into β'' precipitates at 25 °C as a function of Mg to Si ratio of the parent clusters. (a) Molar Gibbs energy. (b) Chemical driving force.

involved in the transformation. Figure 4 shows two possible ways of constructing the driving force value in this situation. In the first case, (a), the evaluation is based on the Gibbs energy versus composition diagram, in the second case, (b), on the extrapolation of the driving force plot from the composition of the particular cluster to the composition of the Mg_5Si_6 phase.

In the construction, an Mg content of 0.3 (mole fraction) is assumed for the hypothetical cluster. The extrapolation is performed via the tangent construction to the curves of the cluster phase at exactly the parent composition and measured as the difference in either molar Gibbs energy or chemical driving force at the composition of the Mg_5Si_6 phase (dashed blue lines). The driving force is read as the difference of Gibbs energy of the β'' phase and the extrapolated curve from the cluster composition. This methodology is explained in more detail, e.g. in [30].

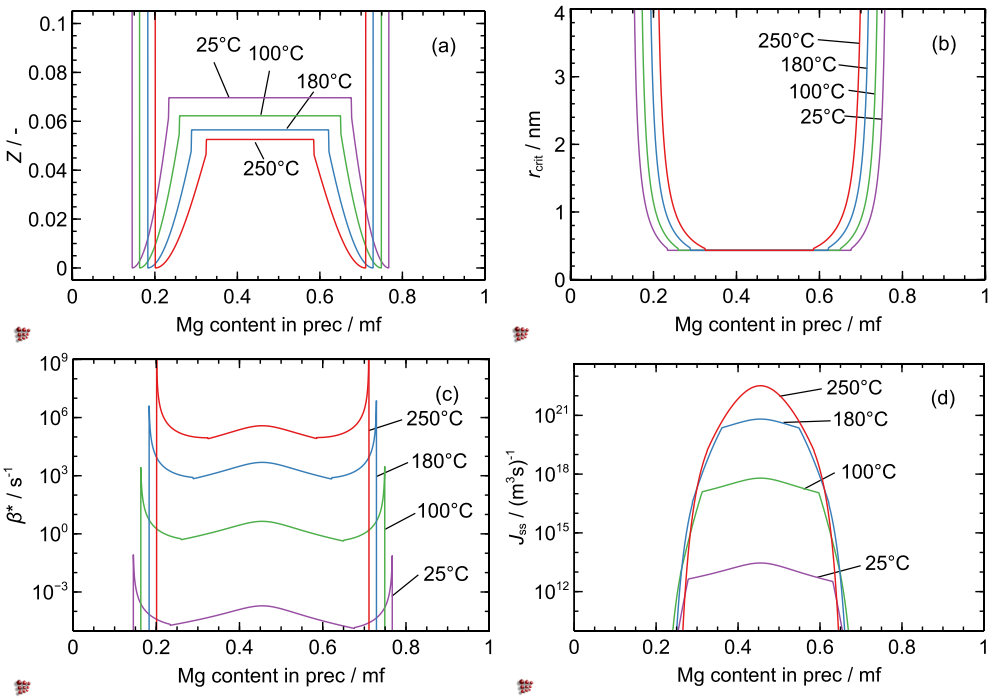

Figure 5. Key quantities for the analysis of the precipitate transformation of clusters into β'' as a function of the Mg–Si ratio of the precipitates. (a) Zeldovich factor, Z, (b) critical nucleation radius, r_{crit}, (c) atomic attachment rate, β^*, (d) steady-state nucleation rate, J_{ss}.

In addition, the plots also show the tangents to the energy and driving force curves passing through the values of the β'' phase, thus embracing the composition range of possible precipitate transformation (dashed light grey lines). The chemical driving force for PT exhibits a maximum at the exact composition of the Mg_5Si_6 phase, with decreasing values for increasing off-stoichiometry.

For the evaluation of the precipitate transformation nucleation rate of β'', some key quantities entering the nucleation rate expression, equation (1), are computed in figure 5 between 25 °C and 250 °C. In figure 5(a), the Zeldovich factor, *Z*, is plotted as a function of the Mg–Si ratio of the parent clusters. As emphasized before, the thermodynamic properties are fully taken from the cluster phase, in accordance with the present assumption that the β'' precipitate nucleates within the cluster phase, and all assumptions of CNT can likewise be applied to the precipitate transformation case. The shape of the Zeldovich factor curve is easily reasoned when comparing with the shape of the critical radius shown in figure 5(b). Since *Z* is related to the curvature of the nucleation energy at the critical radius, see equation (2), *Z* becomes generally larger with a larger critical radius. This effect is responsible for the steep increase of *Z* on the left and right ends of the curves. The increase of *Z* toward the center is due to the increasing chemical driving force (see figure 4(b)) and the accompanying reduction of the critical radius. In the center portion, *Z* exhibits a plateau, which is due to the numerical limitation of the critical radius at 0.35 nm, which is roughly one atomic distance, and which is a default value in MatCalc simulations.

The atomic attachment rate, equation (3), denotes the rate at which atoms attach to the surface of a critical nucleus and it is therefore directly dependent on the size of the critical nucleus. Since the critical size increases with decreasing driving force, β^* increases at the ends of the composition range. On the other hand, the value of β^* is also a function of the composition difference between the nucleus and its surrounding as well as the associated diffusion coefficients. Since the composition difference becomes zero at the exact composition of the β'' precipitate, the curve exhibits a maximum at this point. Importantly, the atomic attachment rate exhibits a strong dependency on temperature. The difference in β^* for the values at 25 °C and 250 °C is roughly nine orders of magnitude. Note that, according to equation (3), β^* has a singularity in the case of identical chemical composition. This is avoided in the present simulations by assuming that a minimum composition difference of at least 1/100 mf must persist at all times.

After evaluation of input quantities for the steady-state nucleation rate, figures 5(a)–(c), and consideration of the size and composition of the parent clusters in the distribution, the steady-state nucleation rate, J_{ss}, is computed and plotted in figure 5(d). Similar to the atomic attachment rate, the nucleation rate shows a strong dependency on temperature. The maximum precipitate transformation rate at room temperature is in the order of 10^{13} $(m^3 s)^{-1}$, while it is 10^{22} $(m^3 s)^{-1}$ at 250 °C. This result conforms to practical experience, which tells that the precipitate transformation at room temperature is very sluggish and clusters remain stable for a rather long time, while the transformation is relatively rapid when increasing the temperature to 180 °C or 250 °C [37].

4.2. Kinetics of cluster-precipitate transformation

For the transformation kinetics from clusters to β'', it is assumed that the transformation rate is mainly controlled by the nucleation process. Once nucleated, the product phase will instantaneously consume the parent and complete the transformation. The kinetics of this process can, thus, be described by the nucleation rate, equation (1), and it is simulated by numerical integration in MatCalc.

The nucleation process is strongly dependent on the distribution of available parent precipitates, both, with respect to size as well as chemical composition. In the present simulations, only one single chemical composition of clusters is considered, which is 0.45 Mg and 0.55 Si (in mol fraction). This composition corresponds roughly to the stoichiometry of the Mg_5Si_6 β'' precipitates. If more than a single composition shall be considered, the treatment of these variants is analogous. It is not further elaborated here, instead, the corresponding simulations are presented and discussed in a follow-up paper.

In the first simulation setup, the evolution of a prescribed distribution of clusters is considered after solutionizing, quenching and natural aging. The simulation of this first part is not actually carried out in the present work, instead, it is assumed that, after the pre-treatment, a normal distribution of clusters (figure 1) is present. The phase fraction of this distribution is assumed to correspond to the metastable equilibrium phase fraction of corresponding clusters at room temperature ($f_{cl} = 0.018$). This assumption ensures that there will occur no further nucleation of clusters during the precipitate transformation and that any independent nucleation of β'' precipitates in the Al matrix is suppressed. The initial size distribution is then heated up to 300 °C with rates between 0.01 and 100 K s^{-1}.

During heating, the precipitate transformation nucleation rate for β'' precipitates is evaluated in each simulation increment based on equation (1). Since the β'' phase is modeled

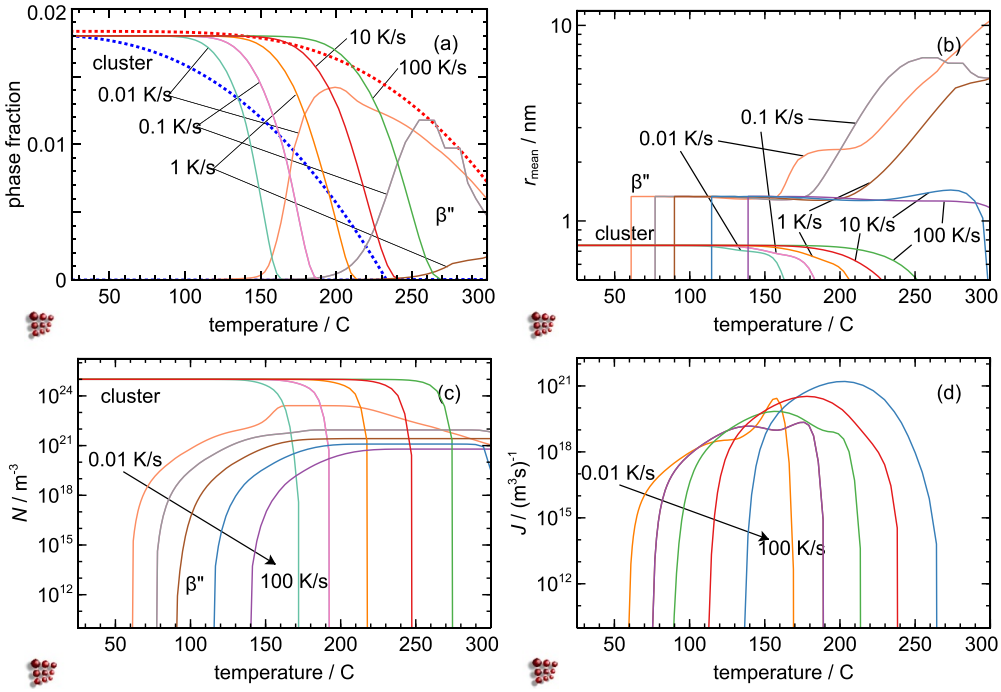

Figure 6. Kinetics of the precipitate transformation of clusters into β'' during continuous heating with 0.01–100 K s^{-1}. (a) Phase fraction, (b) mean radius, r_{mean}, (c) number density, N, (d) transient nucleation rate, J. The dotted lines in (a) denote the equilibrium values for clusters (blue) and β'' (red).

as a line compound, its chemical composition is constant with 4.54 Mg and 5.46 Si (in mf). Although the ratio of Mg and Si is roughly the same in the parent and product phase, in this work, this difference is accounted for as follows: the initial size of the β'' precipitates is evaluated based on the minimum nucleation radius, $r_{min,nucl}$, as defined before. This value is then reduced to account for the actual amount of atoms that are available in the parent precipitate and which can build up the product phase. In the present case, this amounts to roughly 99% of the parent precipitate volume. Although this step is not of large relevance here, it becomes increasingly essential, if the composition of the cluster and β'' deviate more. The 'reduced' radius is finally increased by 20%, which makes the precipitate over-critical and stabilizes the product phase against dissolution after the transformation is carried out in the simulation. This last step is not of large relevance for the evolution of precipitation parameters, mean radius and phase fraction, because the evolution of these is mainly governed by the subsequent growth of the β'' precipitates. It can become relevant, though, in terms of numerical stability of the calculation.

Starting at room temperature with the prescribed distribution of clusters, figure 6 summarizes the evolution of important precipitation parameters during the precipitate transformation for the continuous heating from 25 °C to 300 °C at rates of 0.01, 0.1, 1, 10, and 100 K s^{-1}. The simulation stops when the end temperature is reached.

Figure 6(a) shows the phase fractions of clusters, starting at the initial value of 0.018, which dissolve during heating as expected (compare figure 3). Depending on the heating rate, the dissolution and precipitate transformation are completed between roughly 160 °C and 270 °C. A substantial amount of transformed β'' precipitates is only observed for the slower heating rates between 0.01 and 1 K s^{-1}. Above 1 K s^{-1}, only very few and small β'' precipitates are found, such that the resulting phase fraction remains vanishingly small. Both results are in good qualitative agreement with reversion experiments described by Pogatscher *et al* [38] and Madanat *et al* [39], who observe the extensive precipitate transformation of clusters into β'' at slow heating and dissolution of clusters and suppression of β'' precipitates at sufficiently fast heating.

The evolution of the mean radius of the β'' precipitates, shown in figure 6(b), emphasizes the important influence of the heating rate on the precipitate transformation. At a heating rate of 100 K s^{-1}, some clusters will transform during heating, which is confirmed in the plot of number densities, figure 6(c), however, close to the end temperature of the continuous heating treatment, the mean radius decreases, indicating, that the small β'' precipitates become thermodynamically unstable. At 10 K s^{-1}, the same trend is visible. Initially, the transformed β'' precipitates show a slight increase in their mean radius due to more time at a higher temperature, however, they also become unstable in the end due to the capillarity effect.

At 1 K s^{-1}, the density of β'' precipitates reaches values of $2.5 \cdot 10^{21}$ m^{-3} and a mean radius of roughly 5 nm. This is already sufficiently large to remain stable throughout the simulation. However, the maximum possible phase fraction is not yet reached at 300 °C, which is obvious in comparison with the equilibrium phase fraction plotted as a dashed line in figure 6(a). A further reduction of the heating rate to 0.1 K s^{-1} leads to a completed precipitate transformation already at roughly 150 °C. The maximum phase fraction of β'' precipitates is reached at 250 °C and the mean radius increases to 7 nm. Above this temperature, the radius decreases again and the phase fraction follows approximately the equilibrium line, while the number density remains roughly constant up to 300 °C.

When heating up the cluster distribution with the slowest rate of 0.01 K s^{-1}, the clusters have dissolved/transformed already at 160 °C. This is also the temperature where the number density reaches a maximum of approximately $2.5 \cdot 10^{21}$ m^{-3}, which is almost 100 times more than the maximum at 1 K s^{-1}. Above 200 °C, the phase fraction decreases again, progressing slightly below the equilibrium line due to the capillarity effect that is pronounced for small precipitates. As clearly indicated by the decreasing number density and increasing mean radius, the last stage of the heat treatment is characterized by severe coarsening, ending at a mean radius above 10 nm.

The last plot, figure 6(d), shows the nucleation rates, which are displayed for a better interpretation of the transformation rates. The initial retardation of the precipitate transformation is due to the application of transient nucleation theory, as given by equation (1), and the predicted incubation time, equation (5), which is included in the MatCalc integration algorithm.

Another visualization of the simulation results is presented in figure 7. The left image, (a), shows the evolution of the phase fraction of clusters and β'' precipitates as a function of temperature and heating rates. The right image presents the corresponding mean radii of the two precipitates. The plots show that, at low heating rates, the precipitation of β'' significantly overlaps with the dissolution of the clusters. On the other hand, at high heating rates, the clusters dissolve before they even start to substantially transform into β''. The diagrams also indicate the dependence of the mean radius on the heating rates. At high rates, the radius of β'' remains relatively small due to the short time that is available for precipitate growth. On the other hand, at very slow heating rates, the radius of β'' precipitates increases substantially due to coarsening. Interestingly, there seems to exist a heating rate that produces a maximum phase

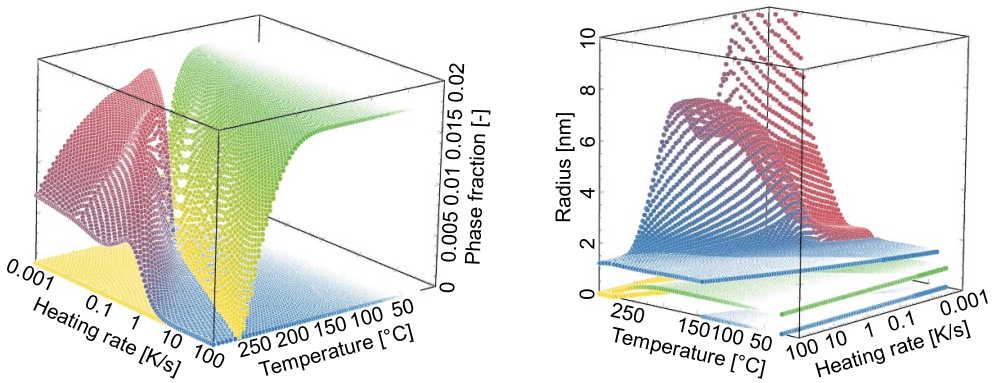

Figure 7. 3D-plots of the precipitate transformation of clusters into β'' during continuous heating as a function of heating rate and temperature. (a) Phase fraction, (b) mean radius. The surface starting at the lowest temperature belongs to the clusters.

fraction of β'' with larger precipitate radii. This indicates already some potential of the present model for optimizing heat treatments in 6xxx Al alloys to achieve, e.g. maximum hardness.

5. Summary

In the present work, a methodology is developed for the direct precipitate transformation of early-stage disordered Mg–Si-rich clusters into β'' in 6xxx Al alloys. The transformation rate is evaluated with transient CNT, where it is assumed that the β'' precipitates nucleate within the clusters. Consequently, all thermodynamic and kinetic quantities are evaluated within the cluster phase. The nucleation rate is evaluated on basis of a minimum size of the β'' nuclei, which is modeled with a smooth nucleation criterion. The following key points are qualitatively included in the presented model:

- The experimental observation that clusters occur in a variety of Mg to Si ratios with varying thermodynamic stability, is fully taken into account in the model formulation.
- The cluster chemistry affects the probability for the transformation calculated in the model, whereas clusters with a composition close to β'' are favored.
- The direct precipitate transformation reaction happens within the cluster phase itself and independent of the matrix phase.

The basic features of the model are investigated in a parameter study assuming an alloy with 1.0 at% Mg and 1.0 at% Si. The simulations capture the qualitative trends according to experimental evidence from the literature reasonably well. They show, for instance, how the heating rate governs the trade-off between cluster dissolution and transformation, resulting in an optimum heating rate with respect to the formation of hardening β'' via the direct precipitate transformation.

Data availability statement

All data that support the findings of this study are included within the article (and any supplementary files).

Acknowledgments

The authors would like to thank the ministry of 'Climate Action, Environment, Energy, Mobility, Innovation and Technology' (BMK), the ministry of 'Digital and Economic Affairs' (BMDW), the Austrian Funding Agency (FFG), as well as the four federal funding agencies Amt der Oberösterreichischen Landesregierung; Steirische Wirtschaftsförderungsgesellschaft m.b.H.; Amt der Niederösterreichischen Landesregierung; Wirtschaftsagentur Wien. Ein Fonds der Stadt Wien for funding project 'We3D' in the framework of the 8th COMET call.

ORCID iDs

Y V Shan https://orcid.org/0000-0002-1254-1117
A Redermeier https://orcid.org/0000-0002-8833-9206
R Kahlenberg https://orcid.org/0000-0002-6281-788X

References

[1] Edwards G A, Stiller K, Dunlop G L and Couper M J 1998 The precipitation sequence in Al-Mg-Si alloys *Acta Mater.* **46** 3893–904
[2] Andersen S J, Zandbergen H W, Jansen J, Træholt C, Tundal U and Reiso O 1998 The crystal structure of the β″ phase in Al-Mg-Si alloys *Acta Mater.* **46** 3283–98
[3] Derlet P M, Andersen S J, Marioara C D and Frøseth A 2002 A first-principles study of the β -phase in Al-Mg-Si alloys *J. Phys.: Condens. Matter* **14** 4011–24
[4] Cayron C and Buffat P A 2000 Transmission electron microscopy study of the β′ phase (Al-Mg-Si alloys) and QC phase (Al-Cu-Mg-Si alloys): ordering mechanism and crystallographic structure *Acta Mater.* **48** 2639–53
[5] Vissers R, van Huis M A, Jansen J, Zandbergen H W, Marioara C D and Andersen S J 2007 The crystal structure of the β′ phase in Al-Mg-Si alloys *Acta Mater.* **55** 3815–23
[6] Dumitraschkewitz P, Gerstl S S A, Stephenson L T, Uggowitzer P J and Pogatscher S 2018 Clustering in age-hardenable aluminum alloys *Adv. Eng. Mater.* **20** 1800255
[7] Poznak A, Marceau R K W and Sanders P G 2018 Composition dependent thermal stability and evolution of solute clusters in Al-Mg-Si analyzed using atom probe tomography *Mater. Sci. Eng.* **721** 47–60
[8] Van Huis M A, Sluiter M H F, Chen J H and Zandbergen H W 2007 Concurrent substitutional and displacive phase transformations in Al-Mg-Si nanoclusters *Phys. Rev.* B **76** 1–6
[9] Andersen S J *et al* 2017 Directionality and column arrangement principles of precipitates in Al-Mg-Si-(Cu) and Al-Mg-Cu linked to line defect in Al *Mater. Sci. Forum* **877** 461–70
[10] Marioara C D, Andersen S J, Hell C, Frafjord J, Friis J, Bjørge R, Ringdalen I G, Engler O and Holmestad R 2024 Atomic structure of clusters and GP-zones in an Al-Mg-Si alloy *Acta Mater.* **269** 119811
[11] Bratland D H, Grong Ø, Shercliff H, Myhr O R and Tjøtta S 1997 Modelling of precipitation reactions in industrial processing *Acta Mater.* **45** 1–22
[12] Khan I N, Starink M J and Yan J L 2008 A model for precipitation kinetics and strengthening in Al-Cu-Mg alloys *Mater. Sci. Eng.* **472** 66–74
[13] Esmaeili S, Lloyd D J and Poole W J 2003 Modeling of precipitation hardening for the naturally aged Al-Mg-Si-Cu alloy AA6111 *Acta Mater.* **51** 3467–81
[14] Milkereit B and Starink M J 2015 Quench sensitivity of Al-Mg-Si alloys: a model for linear cooling and strengthening *Mater. Des.* **76** 117–29
[15] Myhr O R, Grong Ø and Schäfer C 2015 An extended age-hardening model for Al-Mg-Si alloys incorporating the room-temperature storage and cold deformation process stages *Metall. Mater. Trans.* A **46** 6018–39
[16] Myhr O R, Grong Ø and Pedersen K O 2010 A combined precipitation, yield strength, and work hardening model for Al-Mg-Si alloys *Metall. Mater. Trans.* A **41** 2276–89

[17] Lang P, Povoden-Karadeniz E, Falahati A and Kozeschnik E 2014 Simulation of the effect of composition on the precipitation in 6xxx Al alloys during continuous-heating DSC *J. Alloys Compd.* **612** 443–9
[18] Lang P, Wojcik T, Povoden-Karadeniz E, Falahati A and Kozeschnik E 2014 Thermo-kinetic prediction of metastable and stable phase precipitation in Al-Zn-Mg series aluminium alloys during non-isothermal DSC analysis *J. Alloys Compd.* **609** 129–36
[19] Kozeschnik E 2022 Mean-field microstructure kinetics modeling *Encyclopedia of Materials: Metals and Allloys* (Elsevier) pp 521–6
[20] Raabe D *et al* 2022 Making sustainable aluminum by recycling scrap: the science of "dirty" alloys *Prog. Mater. Sci.* **128** 100947
[21] van Huis M A, Chen J H, Sluiter M H F and Zandbergen H W 2007 Phase stability and structural features of matrix-embedded hardening precipitates in Al-Mg-Si alloys in the early stages of evolution *Acta Mater.* **55** 2183–99
[22] Poznak A, Thole V and Sanders P 2018 The natural aging effect on hardenability in Al-Mg-Si: a complex interaction between composition and heat treatment parameters *Metals* **8** 309
[23] Aruga Y, Kozuka M, Takaki Y and Sato T 2014 Evaluation of solute clusters associated with bake-hardening response in isothermal aged Al-Mg-Si alloys using a three-dimensional atom probe *Metall. Mater. Trans.* A **45** 5906–13
[24] Aruga Y, Kozuka M, Takaki Y and Sato T 2015 Formation and reversion of clusters during natural aging and subsequent artificial aging in an Al-Mg-Si alloy *Mater. Sci. Eng.* **631** 86–96
[25] Lukas H L, Fries S G and Sundman B 2007 *Computational Thermodynamics: The Calphad Method* (https://doi.org/10.1017/CBO9780511804137)
[26] Hasting H S, Frøseth A G, Andersen S J, Vissers R, Walmsley J C, Marioara C D, Danoix F, Lefebvre W and Holmestad R 2009 Composition of B″ precipitates in Al-Mg-Si alloys by atom probe tomography and first principles calculations *J. Appl. Phys.* **106** 123527
[27] Kozeschnik E, Svoboda J and Fischer F D 2004 Modified evolution equations for the precipitation kinetics of complex phases in multi-component systems *CALPHAD* **28** 379–82
[28] Kozeschnik E, Svoboda J, Fratzl P and Fischer F D F D 2004 Modelling of kinetics in multi-component multi-phase systems with spherical precipitates II : numerical solution and application *Mater. Sci. Eng.* **385** 157–65
[29] Svoboda J, Fischer F D, Fratzl P and Kozeschnik E 2004 Modelling of kinetics in multi-component multi-phase systems with spherical precipitates I: theory *Mater. Sci. Eng.* **385** 166–74
[30] Kozeschnik E 2013 *Modelling Solid-State Precipitation* (Momentum Press) (https://doi.org/10.5643/9781606500644)
[31] Povoden-Karadeniz E, Lang P, Warczok P, Falahati A, Jun W W W and Kozeschnik E 2013 CALPHAD modeling of metastable phases in the Al-Mg-Si system *CALPHAD* **43** 94–104
[32] Fischer F D, Svoboda J, Appel F and Kozeschnik E 2011 Modeling of excess vacancy annihilation at different types of sinks *Acta Mater.* **59** 3463–72
[33] Lang P, Povoden-Karadeniz E, Mayer W, Falahati A and Kozeschnik E 2013 The bustling nature of vacancies in Al alloys *The 8th Pacific Rim International Congress on Advanced Materials and Processing, TMS (The Minerals, Metals & Materials Society)* ed F Marquis (Wiley) pp 3181–8
[34] Sonderegger B and Kozeschnik E 2009 Generalized nearest-neighbor broken-bond analysis of randomly oriented coherent interfaces in multicomponent Fcc and Bcc structures *Metall. Mater. Trans.* A **40** 499–510
[35] Sonderegger B and Kozeschnik E 2009 Size dependence of the interfacial energy in the generalized nearest-neighbor broken-bond approach *Scr. Mater.* **60** 635–8
[36] Sonderegger B and Kozeschnik E 2010 Interfacial energy of diffuse phase boundaries in the generalized broken-bond approach *Metall. Mater. Trans.* A **41** 3262–9
[37] Pogatscher S, Antrekowitsch H, Leitner H, Ebner T and Uggowitzer P J P J 2011 Mechanisms controlling the artificial aging of Al-Mg-Si alloys *Acta Mater.* **59** 3352–63
[38] Pogatscher S, Antrekowitsch H, Ebner T and Uggowitzer P J 2012 The role of co-clusters in the artificial aging of AA6061 and AA6060 *Light Met.* **2012** 413–20
[39] Madanat M, Liu M and Banhart J 2018 Reversion of natural ageing in Al-Mg-Si alloys *Acta Mater.* **159** 163–72